Anomalous phase behavior of a soft-repulsive potential with a strictly monotonic force

Franz Saija,[1,*] Santi Prestipino,[2,†] and Gianpietro Malescio[2,‡]
[1]*CNR-Istituto per i Processi Chimico-Fisici, Contrada Papardo, 98158 Messina, Italy*
[2]*Dipartimento di Fisica, Università degli Studi di Messina, Contrada Papardo, 98166 Messina, Italy*
(Received 23 July 2009; published 10 September 2009)

We study the phase behavior of a classical system of particles interacting through a strictly convex soft-repulsive potential which, at variance with the pairwise softened repulsions considered so far in the literature, lacks a region of downward or zero curvature. Nonetheless, such interaction is characterized by two length scales, owing to the presence of a range of interparticle distances where the repulsive force increases, for decreasing distance, much more slowly than in the adjacent regions. We investigate, using extensive Monte Carlo simulations combined with accurate free-energy calculations, the phase diagram of the system under consideration. We find that the model exhibits a fluid-solid coexistence line with multiple re-entrant regions, an extremely rich solid polymorphism with solid-solid transitions, and waterlike anomalies. In spite of the isotropic nature of the interparticle potential, we find that among the crystal structures in which the system can exist, there are also a number of non-Bravais lattices, such as *cI*16 and diamond.

DOI: 10.1103/PhysRevE.80.031502 PACS number(s): 64.70.D−, 61.20.Ja, 62.50.−p

I. INTRODUCTION

In typical models of effective pairwise interaction between particles, the repulsive force steadily increases, with an ever-increasing rate, as particles get more and more closer to each other. This behavior, which is typical of, e.g., the Lennard-Jones potential, is originated by the harsh quantum repulsion that is associated with the overlapping of electronic shells. However, effective classical interactions, where the repulsive component undergoes some form of softening in a range of interparticle distances, are relevant for many physical systems. Most of them belong to the realm of the so-called soft matter (solutions of star polymers, colloidal dispersions, microgels, etc.) [1,2] but also the adiabatic interaction potential (electronic in origin) of simple atomic systems under high pressure is manifestly of the soft-core type [3,4].

The effects of particle-core softening on thermodynamic behavior were first investigated by Hemmer and Stell [5], who analyzed the possible occurrence of multiple critical points and isostructural solid-solid transitions. These authors considered pair potentials with a hard core augmented with a finite repulsive component in the form of a square shoulder or a linear ramp, features that may be pertinent to some pure metallic systems, metallic mixtures, electrolytes, and colloidal systems. Few years later, Young and Alder [6] showed that the hard-core plus square shoulder potential gives origin to an anomalous melting line similar to that observed in Cs or Ce. Later, Debenedetti *et al.* [7] showed that systems of particles interacting via potentials whose repulsive core is softened by a curvature change are capable of contracting when heated isobarically (a behavior known as "density anomaly"). More recently, intense investigation of the phase behavior of potentials with a softened core has shown that these models can yield, even for isotropic one-component systems, unusual properties such as a melting line with a maximum followed by a region of re-entrant melting, polymorphism both in the fluid and solid phases, and a rich hierarchy of waterlike anomalies [8–20].

The common feature of all the softened-core potentials investigated so far is that in a range of interparticle distances r, the strength of the two-body force $f(r) \equiv -u'(r)$ reduces or at most remains constant as two particles approach each other, $u(r)$ being the repulsive part of the pair potential. In this interval of distances, $u(r)$ shows a downward or zero concavity, i.e., $u''(r) \leq 0$. Assuming that the repulsion is hard-core-like at small distances and goes to zero sufficiently fast at large distances, the above behavior makes it possible to identify two distinct regions where the repulsive force increases as r gets smaller: an inner region, associated with the impenetrable particle core, and an outer region at large distances. Such potentials are thus endowed with two repulsive length scales: a smaller one ("hard" radius), which is dominant at the higher pressures, and a larger one ("soft" radius), being effective at low pressure. In the range of pressures where the two length scales compete, a system governed by soft-core interactions behaves as a "two-state" system, a simplified viewpoint that nonetheless provides an explanation for re-entrant melting and, in the presence of an additional attractive long-range force, for the existence of a liquid-liquid transition [21].

Though core softening has been usually associated to a repulsive force with a nonmonotonic behavior, the latter condition might be an unnecessary requirement. This observation stems from an analysis of the mathematical expression of core softening, which was put forward by Debenedetti *et al.* [7] under the form $\Delta[rf(r)] < 0$ for $\Delta r < 0$, in some interval $r_1 < r < r_2$, together with $u''(r) > 0$ for $r < r_1$ and $r > r_2$. The above conditions are satisfied if, in the interval (r_1, r_2), the product $rf(r)$ (rather than just f) reduces with decreasing interparticle separation. Hence, the core-softening property may also be satisfied with a strictly convex potential, yielding a repulsive force which everywhere increases for decreasing r, provided that in a range of interparticle distances,

*Corresponding author. saija@me.cnr.it
†santi.prestipino@unime.it
‡malescio@unime.it

the increasing rate of $f(r)$ be sufficiently small. On this basis, we expect that the class of core-softened potentials is in fact much wider than thought before.

We hereafter study the phase diagram of a model potential which is soft, according to Debenedetti's formulation, though being characterized by a *strictly monotonic* force for all distances [i.e., $u''(r)>0$ everywhere]. We find that this potential exhibits the whole spectrum of anomalies that are usually associated with soft-core potentials, including re-entrant melting regions, solid polymorphism, and waterlike anomalies. This paper is organized as follows. In Sec. II, we describe the model system, which is the subject of our investigation. In Sec. III, we outline the simulation method that is used to map out the phase diagram. The simulation results are presented and discussed in Sec. IV, while further remarks and conclusions are postponed to Sec. V.

II. MODEL

We consider a purely repulsive pair potential modeled through an exponential form, first introduced, about four decades ago, by Yoshida and Kamakura (YK) [22],

$$u(r) = \epsilon \exp\left\{ a\left(1-\frac{r}{\sigma}\right) - 6\left(1-\frac{r}{\sigma}\right)^2 \ln\left(\frac{r}{\sigma}\right)\right\}, \qquad (1)$$

where ϵ and σ are the energy and length units, respectively, and $a>0$. This potential behaves as r^{-6} for small r and falls off very rapidly for large r. The softness of the repulsion is controlled by the a parameter. When $a<1.9$, the YK potential has a region with downward curvature, where the force decreases as two particles get closer.

Approximate theoretical calculations [22] suggest that the melting line of the YK potential might display a re-entrant melting region for values of a that are larger than 1.9, i.e., even when no downward concavity is present. In order to explore this possibility and discuss it in relation with other anomalous behaviors, we have investigated the phase behavior of the YK potential for $a=2.1$ through numerical simulation. For this a value (as well as for all a's falling in the range 1.9–2.3) $u(r)$ is strictly convex (see Fig. 1), i.e., its second derivative is positive everywhere; hence the repulsive force is strictly increasing for decreasing r, at variance with the core-softened potentials considered so far. However, the rate at which the force increases is not monotonous. By the way, in a range of r that roughly corresponds to the local minimum of $u''(r)$, the repulsive force increases with decreasing r much more slowly than in the adjacent regions, in such a way that the Debenedetti core-softening property is still satisfied.

III. METHOD

A major problem, when drawing the phase diagram of a model system of particles interacting through an assigned potential, is to identify the solid phases. This is a critical issue for soft-core repulsions since experience has shown that many different crystal structures are stabilized for such systems upon varying the pressure [4,16,19,23]. In the present study, we consider as candidates for the solid phase

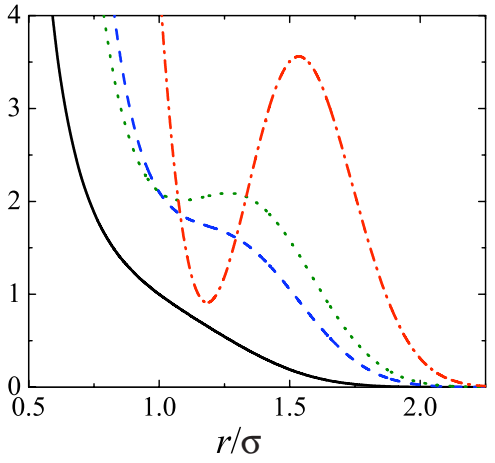

FIG. 1. (Color online) Yoshida-Kamakura potential $u(r)$ for $a=2.1$ (black solid line, expressed in ϵ units), two-body force $f(r)=-u'(r)$ (blue dashed line, ϵ/σ units), product $rf(r)$ (green dotted line, ϵ units), and second derivative of the potential $u''(r)$ (red dash-dotted line, ϵ/σ^2 units).

precisely those crystal structures that a previous investigation of the same potential [4] showed to be stable at zero temperature. These include the face-centered cubic (fcc), body-centered cubic (bcc), and simple hexagonal (sh) lattices, as well as a number of non-Bravais lattices, i.e., the A7, diamond, A20, and hexagonal close-packed (hcp) lattices. On increasing pressure, each of these structures gives, in turn, the most stable structure at $T=0$. The sequence of stable crystals for increasing pressures was found to be [4]

$$\mathrm{fcc} \xrightarrow{0.63} \mathrm{bcc} \xrightarrow{1.26} \mathrm{sh} \xrightarrow{2.29} \mathrm{A7} \xrightarrow{2.55} \mathrm{diamond} \xrightarrow{4.91} \mathrm{sh} \xrightarrow{5.46} \mathrm{A20} \xrightarrow{12.07} \mathrm{hcp} \xrightarrow{15.68} \mathrm{bcc} \xrightarrow{52.75} \mathrm{fcc} \xrightarrow{138.28} \mathrm{hcp} \xrightarrow{365.65} \mathrm{fcc}, \qquad (2)$$

where the numbers above the arrows indicate the transition pressures expressed, to within a precision of 0.01, in units of ϵ/σ^3. Where pertinent, the values of the internal parameters of the phases listed in Eq. (2) are reported in Ref. [4]. Although the above sequence of phases resulted from a careful scrutiny of about 30 crystal structures, we cannot exclude that some relevant structures might have been overlooked. In general, we may expect that the same crystals that are stable at $T=0$ also give the underlying lattice structure for the solid phases at $T>0$. Anyway, if more crystals exist at $T=0$ with nearly the same chemical potential μ in a pressure range, each of them represents a potentially relevant solid phase. In our case, this occurs for $P\approx 2.4$, where the ground state is of A7 type but some $oC8$ and $cI16$ crystals have only slightly larger chemical potentials. Hence, we include also these lattices in our list of solid candidates.

We calculate the phase diagram of the YK model for $a=2.1$ by performing Monte Carlo (MC) simulations in the isothermal-isobaric NPT ensemble (i.e., at constant temperature T, pressure P, and number N of particles), as well as in the canonical NVT ensemble, using the standard Metropolis algorithm with periodic boundary conditions and the nearest-image convention. In the solid phases, the number of par-

ticles is chosen so as to guarantee a negligible contribution to the interaction energy from pairs of particles separated by half the minimum simulation-box length. With this choice, we checked in a number of cases that the exact location of phase boundaries is only negligibly affected by the finite size of the sample. More precisely, our samples consisted of 500 particles in the fcc phase, of 432 particles in the bcc phase, of 800 particles in the sh phase, of 512 particles in the diamond phase, of 1024 particles in the *cI*16 phase, of 1152 particles in the A7 phase, and of 768 particles in the *oC*8 phase. Depending on the solid phase with which the fluid is compared to in order to assess its relative stability, we consider fluid samples of 500–800 particles. At given T and P, sample equilibration typically took from 20 000 to 50 000 MC sweeps, a sweep consisting of one average attempt per particle to change its position plus (for the *NPT* case only) one attempt to change the volume through a rescaling of particle coordinates. The maximum random displacement of a particle and the maximum volume change in a trial MC move are adjusted every sweep during the equilibration run so as to obtain an acceptance ratio of moves close to 50% (afterward, during the production session, they are maintained fixed). Thermodynamic averages are computed over trajectories from 3×10^4 to 10^5 sweeps long.

In a typical *NPT* simulation, we generate a sequence of simulation runs along an isobar, starting from the cold solid on one side and from the hot fluid on the other side (a chain of *NVT* runs along an isotherm at a sufficiently high temperature provides the link to a dilute-fluid state). The last configuration produced in a given run is taken to be the first of the next run at a slightly different temperature. The starting configuration of a "solid" chain of runs is a low-temperature perfect crystal whose density is set equal to its $T=0$ value at that pressure. In the case of a structure with internal parameters, the same $T=0$ optimal parameters are chosen in the preparation of the crystal sample. Usually, a series of runs is continued until a sudden change is found in the difference of energy/volume between the solid and the fluid, so as to avoid averaging over heterogeneous thermodynamic states. The density of a solid phase ordinarily varies very little with increasing temperature along an isobar. A sudden density change thus indicates a mechanic instability of the solid in favor of the fluid; hence it signals the approximate location of melting. In fact, this so-called "heat-until-it-melts" (HUIM) procedure allows to locate the maximum overheating temperature T_m', which may however be substantially higher than the fluid-solid coexistence temperature T_m.

In order to compute the difference in chemical potential between any two equilibrium states of the system (say, 1 and 2) belonging to the same phase, we use the standard thermodynamic-integration method. This allows to obtain a thermodynamic potential as an integral over the simulation path of a calculated statistical average (energy, density, or pressure, depending on the path followed). To be specific, we use

$$f_{\rm ex}(T,\rho_2)-f_{\rm ex}(T,\rho_1)=k_BT\int_{\rho_1}^{\rho_2}\frac{d\rho}{\rho}\left(\frac{P(T,\rho)}{\rho k_BT}-1\right) \quad (3)$$

along an isothermal *NVT* simulation path, $f_{\rm ex}$ being the excess Helmholtz free energy, while we use the formulas

$$\mu(T,P_2)-\mu(T,P_1)=\int_{P_1}^{P_2}dPv(T,P) \quad (4)$$

and

$$\frac{\mu(T_2,P)}{T_2}-\frac{\mu(T_1,P)}{T_1}=-\int_{T_1}^{T_2}dT\frac{u(T,P)+Pv(T,P)}{T^2} \quad (5)$$

along an isothermal and isobaric *NPT* path, respectively, u and v being the specific values of energy and volume. To prove useful, the above equations require an independent estimate of $f_{\rm ex}$ or μ in one reference state for each phase. For the fluid, a reference state can be any state being characterized by a very small system density since then the excess chemical potential can be accurately estimated through Widom's particle-insertion method [24]. In order to calculate the excess Helmholtz free energy of a solid, we resort to the Frenkel-Ladd method [25] (see Ref. [26] for a full description of the method and of its implementation on a computer). The solid excess Helmholtz free energy is calculated through a series of *NVT* simulation runs at a fixed state point, i.e., for fixed density and temperature.

IV. RESULTS AND DISCUSSION

We arbitrarily restrict our analysis of the phase diagram to pressures P smaller than 5 (in reduced units), which corresponds approximately to the upper limit of stability of the diamond crystal at $T=0$ [4]. For a number of pressures, we first calculate the fluid-solid coexistence temperature T_m by employing the "exact" free-energy method described above. By estimating the maximum overheating temperature T_m' through the HUIM method, we find that the difference between $T_m'(P)$ and $T_m(P)$ is always small in relative terms (less than 15%) and is significant only at the highest pressures P. Hence, we use the more rapid HUIM approach to derive the overall trend of the melting line. The investigated system shows a rich solid polymorphism at $T>0$ (see Fig. 2), which is closely related to the alternation of crystal phases at zero temperature. In the low-pressure region ($P<1$), upon increasing pressure at low temperatures ($T<0.04$, in ϵ/k_B units) the fluid freezes first into a fcc solid, which then undergoes a transition into a bcc solid. At higher temperatures, in a narrow T interval, the sequence of phase transitions undergone by our system with increasing pressures is fluid-bcc-fcc-bcc. This behavior is similar to that observed for the Gaussian core model [27] and occurs from $T_{\rm tr}$ to $T\simeq0.05$, $T_{\rm tr}\lesssim0.045$ being the fluid-bcc-fcc triple-point temperature. For $0.05<T<0.06$, the fcc phase ceases to be stable and the fluid freezes directly into a bcc solid. The bcc-fluid coexistence line shows, at $P\simeq0.6$, a maximum melting temperature; above this pressure, the dT/dP slope of the bcc melting line is negative. Thus, the bcc solid undergoes, for not too low temperatures, re-entrant melting into a denser fluid.

At low temperatures, the bcc solid transforms, for pressures around 1.3, into a solid with a sh structure. Hence, there should be a fluid-bcc-sh triple point, which terminates the bcc re-entrant melting line. This is illustrated in detail in

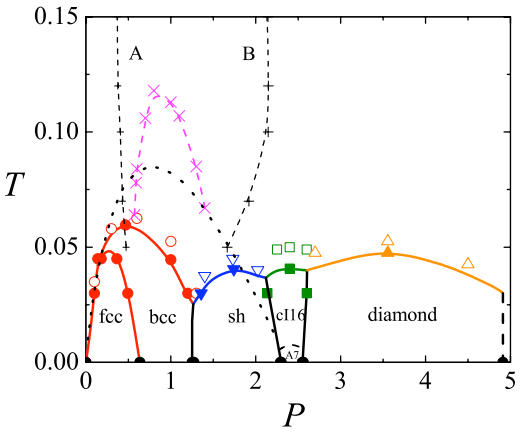

FIG. 2. (Color online) Phase diagram of the Yoshida-Kamakura interaction model ($a=2.1$). Pressure P and temperature T are expressed in units of ϵ/σ^3 and ϵ/k_B, respectively (k_B being Boltzmann's constant). The phase-transition points obtained by exact free-energy calculations are represented as full symbols (different colors refer to different solid structures; errors are smaller than the size of the symbols). The data points lying on the $T=0$ axis are exact solid-solid boundaries [7]. The solid lines through the transition points are tentative phase boundaries drawn following the trend of thresholds of maximum solid overheating, hereby reported as open dots. The location of the dashed line delimiting the A7 region from the above is uncertain since we did not carry out any exact free-energy calculation for the A7 solid. The dashed line connecting crosses is the locus of density maxima in the fluid phase. Curves A and B connect points of maximum and minimum values of $-s_2$, respectively (see Fig. 6). The open region between A and B is the structurally anomalous region. The black dotted line is the melting line as estimated in [22]. All lines in the figure are guides for the eyes.

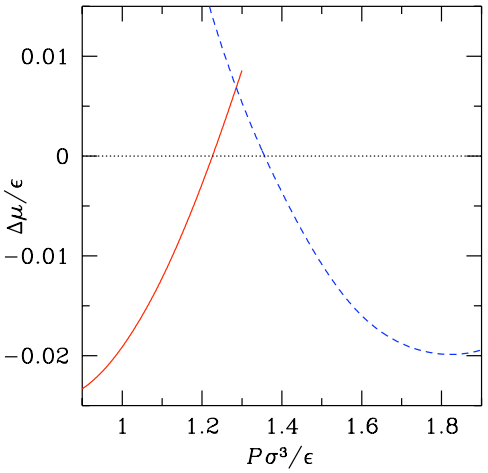

FIG. 3. (Color online) Chemical potential μ of the bcc and sh solids at $T=0.03$, taking the fluid phase as reference: bcc (solid red line), sh (dashed blue line), and fluid (dotted line). The stable phase is the one with lower μ, hence, the equilibrium system is fluid between 1.226 (bcc-fluid transition pressure) and 1.357 (fluid-sh transition pressure). Note the existence of a minimum in the μ difference between sh and fluid at $P\simeq 1.8$, which roughly corresponds to the pressure at which the sh melting temperature is maximum.

Fig. 3, where we show the calculated chemical potentials of the three phases along the $T=0.03$ isotherm. Upon further increasing pressure, a $cI16$ solid with internal parameter $x=0.125$ becomes stable (see Ref. [4] for a definition of x). This can occur only for high enough T since, in the pressure interval $2.30<P<2.55$, a certain A7 crystal has a lower chemical potential than $cI16$ at $T=0$ (we have checked that no $oC8$ solid is stable in the same temperature range). In other words, a small A7 basin exists below $T\approx 0.01$. Following the $cI16$ phase, another solid phase arranged according to the diamond structure becomes stable in a broad pressure range, starting from $P\simeq 2.6$.

Within the precision of our calculation, the overall melting line exhibits, in addition to the first (bcc-fluid) re-entrant region, other portions with negative dT/dP slope, though less pronounced than the first. The alternation of solid phases at low temperatures goes on beyond $P=5$ until, eventually, the system sets in a fcc solid that coexists with the fluid phase at arbitrary high temperatures, the coexistence line becoming asymptotically the same as for the r^{-6} potential. The complex phase behavior shown in Fig. 2 is absent in the theoretical calculation of Yoshida and Kamakura [22], where only the possibility of a fcc solid was taken into account. With this limitation, only one region of re-entrant melting is predicted and the high-pressure fluid can be stable even at zero temperature. Moreover, the height and width of the low-density solid region are largely overestimated by the theory as compared to the simulation results here presented.

Our results show that the model system here considered, though described by a spherically symmetric potential, can exist under the form of stable non-Bravais crystals. The rich polymorphism observed follows from the peculiar dependence of the interatomic force with distance, which leads to the existence of two incommensurate length scales. In the pressure and temperature regimes, where these lengths compete with each other, compact arrangements such as the fcc and bcc lattices are frustrated and low-coordinated arrangements are preferred. Our results are relevant for those physical systems that are characterized by a certain softness of the repulsive interaction. These include intrinsically soft materials, such as colloids, polymers, etc., but also atomic systems at extremely high pressures. Phase diagrams with solid polymorphism and multiple re-entrant melting have been observed at high pressures in some elements such as Sr [28] and predicted by *ab initio* simulation for others [29]. Concerning model systems, a phase behavior with features similar to those noted above was found for the hard-core plus repulsive step potential [16] and for Hertzian spheres [19].

Some insight into the mechanisms that give origin to the complex phase behavior observed can be got from analyzing the radial distribution function $g(r)$. We computed $g(r)$ for various pressure values, at a temperature slightly larger than the maximum melting temperature $T_M\simeq 0.06$ of the bcc solid (Fig. 4). At very low pressure, the first peak of $g(r)$ is centered around $r\lesssim 2$ (in units of σ). As P increases up to $P\approx 0.50$, this peak moves upward while its position shifts toward $r\simeq 1.5$. For further pressure increase, its height decreases while its position remains almost unaltered. At the same time, a new peak develops around $r=1$, whose height grows with P. This behavior is significantly different from

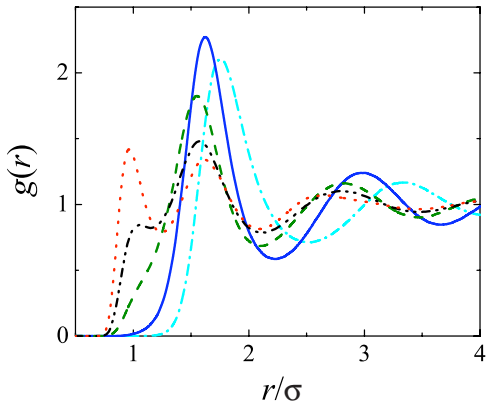

FIG. 4. (Color online) Pair distribution function $g(r)$ for $T=0.07$: $P=0.15$ (cyan dash-dotted line); $P=0.49$ (blue solid line); $P=0.99$ (green dashed line); $P=1.56$ (black dash-dot-dotted line); and $P=3.02$ (red dotted line).

that of simple fluids, where all peaks of $g(r)$ get higher with pressure when keeping T constant, and is consistent with the gradual penetration of particles inside the inner core. Thus, the analysis of $g(r)$ points to the existence of two competitive scales of nearest-neighbor distance, i.e., a larger soft length fading out with increasing pressure in favor of the smaller hard length. The soft-repulsive distance falls approximately at $r=1.5$, which is where the second derivative of the potential has a local maximum, while the hard length scale remains defined by the extremely rapid increase in the short-range repulsive force around $r=1$.

Thermodynamic, dynamic, and structural anomalies have been observed in a number of substances (such as water, silica, silicon, carbon, and phosphorous) [21]. These unconventional features are usually referred to as waterlike anomalies. Although these substances are all characterized by local tetrahedral order, in the last years waterlike anomalies have been found also in systems with spherically symmetric potentials, provided that the repulsion is of the softened-core type [8–20] In order to investigate the existence of anomalies in our system, we first analyzed the behavior of the number density in the fluid phase above the melting line. We find that in the region lying approximately above the re-entrant portion of the bcc-fluid coexistence line, decreasing temperature at constant pressure leads first to a density increase and then—contrary to standard behavior—to a density decrease for further cooling (Fig. 5). The anomalous behavior of the density can be interpreted in terms of the existence of two repulsive length scales: as T reduces at constant pressure, the larger soft scale becomes favored with respect to the smaller hard one. Thus, compact local structures are less favored than open ones, which causes a decrease in the number of particles within a given volume. The P-T region where the density behaves anomalously is bounded from the above by the locus of points where the density attains its maximum value, i.e., by the temperature of density maximum (TMD) line, while its lower bound is the limit of stability of the fluid phase, namely, the bcc-fluid coexistence line (see Fig. 2). Within the region of density anomaly, the system expands upon cooling under fixed pressure. Consistently, the thermal-expansion coefficient $\alpha_P=(1/V)(\partial V/\partial T)_P$ is negative, vanishing along the TMD line (Fig. 5).

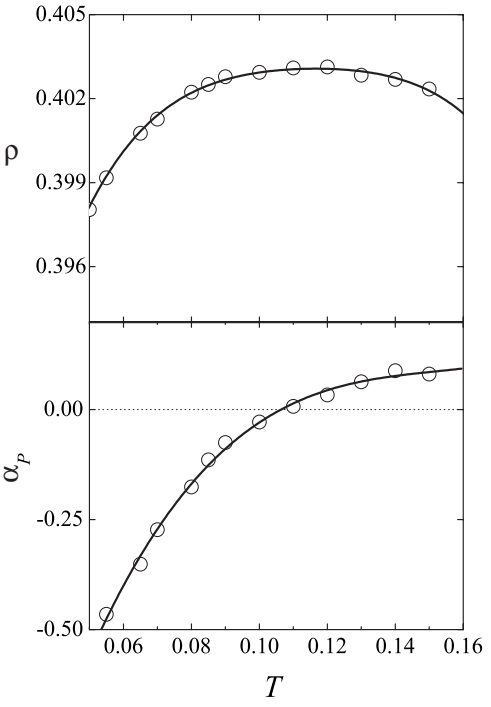

FIG. 5. Reduced number density ρ (upper panel) and thermal-expansion coefficient α_P (lower panel) plotted as a function of temperature for $P=1$. The solid lines are polynomial fits of the data. Note that α_P vanishes approximately where ρ is maximum.

A series of studies have shown that thermodynamic (and dynamic) anomalies are strongly correlated with anomalous trends in the structural order of the system [30]. A measure of this quantity is provided by the pair entropy per particle,

$$s_2 = -\frac{k_B}{2}\rho \int d^3r[g(r)\ln g(r) - g(r) + 1], \tag{6}$$

which describes the contribution of two-body spatial correlations to the excess entropy of the fluid [31]. For a completely uncorrelated system, $g(r)=1$ and then $s_2=0$. For systems with a long-range order, spatial correlations persist over large distances and s_2 become large and negative. Thus, $-s_2$ can be taken as an indicator of structural order. This parameter yields information about the average relative spacing of the particles, i.e., it describes the tendency of particle pairs to adopt preferential separations. In the investigated system, the structural order initially increases upon compression (Fig. 6), similarly to simple fluids. However, as pressure is further increased, $-s_2$ attains a maximum value and then decreases, i.e., the fluid loses structural order upon compression (structural anomaly). At sufficiently high density, after attaining a local minimum, $-s_2$ recovers a normal trend, increasing monotonously with pressure. Upon increasing the temperature, the structural anomaly becomes less and less marked (i.e., the difference between the local extrema of $-s_2$ gets smaller). As seen in Fig. 2, the region where the fluid has a structurally anomalous behavior embraces the density anomaly region; a similar relationship between the structural and density anomalies holds for water and for a number of model systems [30,32–34].

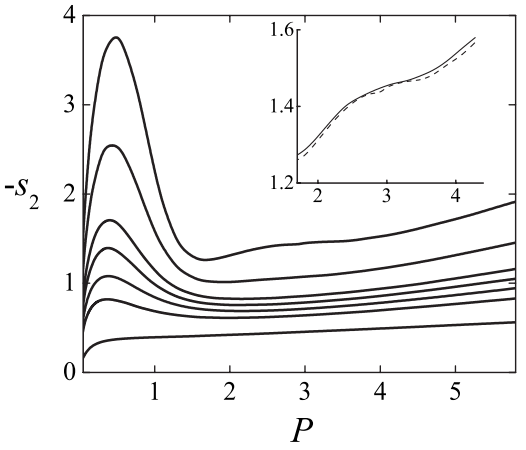

FIG. 6. Structural order parameter $-s_2$ plotted for $N=500$ as a function of the reduced pressure at different temperatures: from top to bottom, $T=0.05$, 0.07, 0.1, 0.12, 0.15, 0.2, and 0.50. The inset shows a magnification of $-s_2$ for $T=0.05$ (dashed line: $N=500$; solid line: $N=800$).

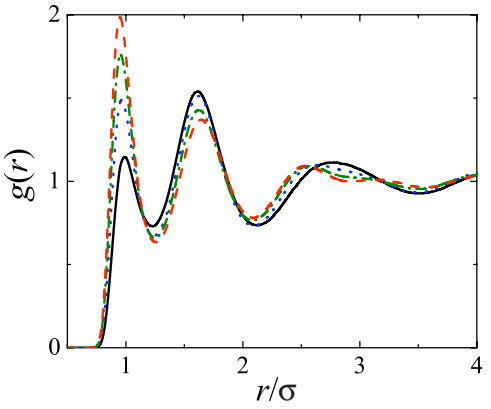

FIG. 7. (Color online) Pair distribution function $g(r)$ for $T=0.05$: $P=1.95$ (black solid line); $P=2.75$ (blue dotted line); $P=3.67$ (green dash-dotted line); and $P=4.71$ (red dashed line).

Though, from a thermodynamic point of view, phase coexistence is determined solely by the equality of the Gibbs free energy in the two phases, an incoming phase transition may induce a number of modifications in the involved phases (the analysis of such changes provides the basis for the so-called "one-phase" criteria for phase transitions). Here, we investigate to what extent the rich solid polymorphism shown by our system at low temperature is reflected in the fluid lying at higher temperatures. The structural order, as measured by $-s_2$, offers interesting insight about this point. The behavior of $-s_2$ shows that the low-density bcc region casts an imprint on the surrounding fluid, under the form of a marked increase in the structural order near the pressure of maximum melting temperature of the solid. On the contrary, the detailed shape of the melting curve at intermediate densities does not significantly affect the structural order of the fluid, which shows a steady enhancement with pressure. In order to observe an appreciable modification of this behavior, it is necessary to examine the fluid very close to the solid. Only the lowest $-s_2$ isotherm at $T=0.05$, i.e., just at the lower edge of the fluid phase, shows a modest bump reflecting the fine details of the melting line (see Fig. 6). These results suggest that the influence of low-coordinated solid structures on the structural order of the neighboring fluid is much weaker than for compact lattices. From the analysis of the $g(r)$, it clearly appears that the soft-repulsive scale looses efficacy in the pressure range corresponding approximately to the re-entrant region of the bcc solid, where both density and structural anomalies occur. Beyond $P=1.5$, the second peak of $g(r)$ changes only slightly (decreasing with increasing density), while the first peak builds up significantly with pressure, which is the main reason for the steady increase in $-s_2$ at intermediate pressures (this is related to the gradual increase in local order with compression, until the fluid crystallizes into a fcc structure at very high pressures, out of the range shown in Fig. 2). The third peak undergoes, with increasing pressure, subtle but significant changes, splitting in two minor peaks (Fig. 7). Such changes mirror the alternation of the solid structures at low T but, being small modifications of the $g(r)$, they scarcely affect the structural order of the fluid, at least that quantified by $-s_2$.

V. CONCLUDING REMARKS

The occurrence of anomalous phase behavior within the class of isotropic one-component classical potentials was, up to now, thought to be possible only for potentials with a region of downward or zero curvature, where the repulsive force decreases or is at most constant as two particles get closer. Here, we have shown that anomalous phase behaviors can actually occur also for a system of particles interacting through a strictly monotonic repulsive force provided that in a range of interparticle distances the force increases more slowly, with decreasing r, than in the adjacent regions. This condition gives origin, in spite of the convexity of the potential, to two distinct repulsive length scales, a feature that seems instrumental for the occurrence of re-entrant melting and the related waterlike anomalies. From the present results, we may expect that the real systems effectively characterized by isotropic interactions and able to show that unusual phase behaviors are more numerous than previously believed.

[1] C. N. Likos, Phys. Rep. **348**, 267 (2001).
[2] C. N. Likos, Soft Matter **2**, 478 (2006).
[3] G. Malescio, F. Saija, and S. Prestipino, J. Chem. Phys. **129**, 241101 (2008).
[4] S. Prestipino, F. Saija, and G. Malescio, Soft Matter **5**, 2795 (2009).
[5] P. C. Hemmer and G. Stell, Phys. Rev. Lett. **24**, 1284 (1970).
[6] D. A. Young and B. J. Alder, Phys. Rev. Lett. **38**, 1213 (1977);

J. Chem. Phys. **70**, 473 (1979).
[7] P. G. Debenedetti, V. S. Raghavan, and S. S. Borick, J. Phys. Chem. **95**, 4540 (1991).
[8] F. H. Stillinger, J. Chem. Phys. **65**, 3968 (1976).
[9] M. R. Sadr-Lahijany, A. Scala, S. V. Buldyrev, and H. E. Stanley, Phys. Rev. Lett. **81**, 4895 (1998).
[10] E. A. Jagla, J. Chem. Phys. **111**, 8980 (1999).
[11] P. Kumar, S. V. Buldyrev, F. Sciortino, E. Zaccarelli, and H. E. Stanley, Phys. Rev. E **72**, 021501 (2005).
[12] L. M. Xu, S. V. Buldyrev, C. A. Angell, and H. E. Stanley, J. Chem. Phys. **130**, 054505 (2009).
[13] A. Barros de Oliveira, P. A. Netz, T. Colla, and M. C. Barbosa, J. Chem. Phys. **124**, 084505 (2006).
[14] H. M. Gibson and N. B. Wilding, Phys. Rev. E **73**, 061507 (2006).
[15] E. Lomba, N. G. Almarza, C. Martin, and C. McBridge, J. Chem. Phys. **126**, 244510 (2007).
[16] D. Yu. Fomin, N. V. Gribova, V. N. Ryzhov, S. M. Stishov, and D. Frenkel, J. Chem. Phys. **129**, 064512 (2008).
[17] A. B. de Oliveira, G. Franzese, P. A. Netz, and M. C. Barbosa, J. Chem. Phys. **128**, 064901 (2008).
[18] O. Pizio, H. Dominguez, Y. Duda, and S. Sokolowski, J. Chem. Phys. **130**, 174504 (2009).
[19] J. Pàmies, A. Cacciuto, and D. Frenkel, J. Chem. Phys. **131**, 044514 (2009).
[20] G. J. Pauschenwein and G. Kahl, J. Chem. Phys. **129**, 174107 (2008).
[21] P. F. McMillan, J. Mater. Chem. **14**, 1506 (2004).
[22] T. Yoshida and S. Kamakura, Prog. Theor. Phys. **47**, 1801 (1972); **52**, 822 (1974); **56**, 330 (1976); S. Kamakura and T. Yoshida, *ibid.* **48**, 2110 (1972).
[23] C. N. Likos, N. Hoffmann, H. Löwen, and A. A. Louis, J. Phys.: Condens. Matter **14**, 7681 (2002).
[24] B. Widom, J. Chem. Phys. **39**, 2808 (1963).
[25] D. Frenkel and A. J. C. Ladd, J. Chem. Phys. **81**, 3188 (1984); see also J. M. Polson, E. Trizac, S. Pronk, and D. Frenkel, *ibid.* **112**, 5339 (2000).
[26] S. Prestipino and F. Saija, J. Chem. Phys. **126**, 194902 (2007).
[27] S. Prestipino, F. Saija, and P. V. Giaquinta, Phys. Rev. E **71**, 050102(R) (2005).
[28] D. Errandonea, R. Boehler, and M. Ross, Phys. Rev. B **65**, 012108 (2001).
[29] A. A. Correa, S. A. Bonev, and G. Galli, Proc. Natl. Acad. Sci. U.S.A. **103**, 1204 (2006).
[30] J. R. Errington and P. G. Debenedetti, Nature (London) **409**, 318 (2001).
[31] R. E. Nettleton and M. S. Green, J. Chem. Phys. **29**, 1365 (1958).
[32] R. Esposito, F. Saija, A. M. Saitta, and P. V. Giaquinta, Phys. Rev. E **73**, 040502(R) (2006).
[33] Z. Yan, S. V. Buldyrev, N. N. Giovambattista, and H. E. Stanley, Phys. Rev. Lett. **95**, 130604 (2005).
[34] Z. Yan, S. V. Buldyrev, N. N. Giovambattista, P. G. Debenedetti, and H. E. Stanley, Phys. Rev. E **73**, 051204 (2006).